Single Crystal Silicon (SCS) MicroMirror Arrays using Deep Silicon Etching and IR Alignment

Chris S.B. Lee, Russell Y. Webb, John M. Chong and Noel C. MacDonald
School of Electrical Engineering
Cornell University, Ithaca NY14853
aloha@ee.cornell.edu

Abstract

10 x 10 and 5 x 5, a high mirror fill factor (> 70 %), low voltage operation (< 30 V), single crystal silicon (SCS) micromirror arrays have been designed, fabricated, and tested. Each mirror is 320 μm by 170 μm and is individually addressable. In comparison to thin film micro-mirror arrays [1,2], the SCS mirror surface is optically flat and smooth, free of residual stress, and highly reflective after the deposition of a thin aluminum layer. In addition to a flat mirror, high-aspect-ratio grating structures have been fabricated on the surface of the mirrors, enhancing the optical manipulation potential of devices.

Introduction

The design and fabrication of the mirror array rely on a through-the-wafer etch (Bosch process – PlasmaTherm SLR-770) and a front-to-back infrared (IR) alignment. The SCS integrated two-depth actuators are fabricated on one side of a double polished wafer, and the mirror structures are fabricated on the other side. The actuator on the front is connected to the backside mirror by a rigid post. Three masks are required. The cross-section of a through-the-wafer, SCS micromirror structure is shown in Figure 1. The through-the-wafer etch releases the 320 μm by 170 μm mirror platform; the suspension of movable structures is provided by springs from the actuators that are connected to the substrate anchors. Two mirror designs are presented for micro-optics applications: a pure z-motion and a torsional tilt motion.

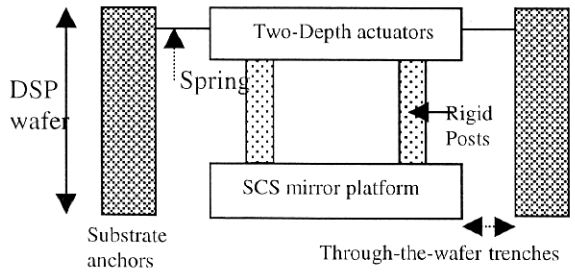

Figure 1. Cross-sectional schematics of through-the-wafer, SCS micromirror array.

The theory of electrostatic comb-drive levitation was first investigated by Tang et al [3]. Electrostatic torsional motion for SCREAM comb drives has been reported [4,5]. The asymmetric electric field distribution in SCREAM beams is attributable to the following three geometrical effects: (1) The presence of a grounded plane underneath the fingers contributes to a net vertical force induced on the movable comb fingers. (2) The difference in the electrode heights increases the vertical asymmetry in the electric field. (3) The asymmetric metal coverage on the SCREAM beam increases the net electric field. This is mainly due to the difference in metal coverage between the top of the beam and the bottom of the beam where the oxide overhang isolates the metal from the silicon core [6]. Cross-sectional schematics of the asymmetric electric field lines created by applying a positive voltage to the fixed fingers and grounding the movable fingers and the substrate are shown in Figure 2. Asymmetric electric field distribution results in the out-of-plane actuation force.

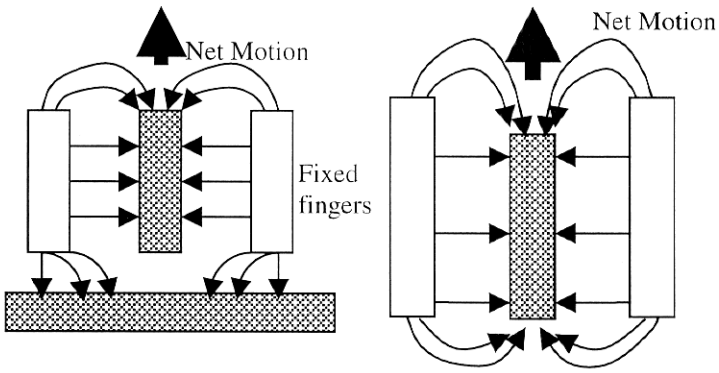

Figure 2. (a) The same height electrode. (b) Two-depth electrodes for a SCS micromirror array. The out-of-plane motion is enhanced due to greater fringing field effects. The substrate is far away from the fingers.

The fabrication scheme of the mirror array requires that the substrate is very far away from the electrodes (> 40 μm). In this case, the vertical electric field distribution arises from the asymmetric coverage of the aluminum layer and the electrode height differences. To simulate the torque generated by the two-depth electrode design,

the electrostatic simulations were done using COULOMB, a three-dimensional boundary element modeler. The geometry for the simulated device is given as follows: a finger height of 20 μm, a finger width of 1 μm, a finger gap of 2 μm, and a height difference of 0.3 μm. The substrate ground plane is placed infinitely far away. One movable finger between two fixed fingers is simulated. The fingers are assumed to be perfect conductors in the simulation. A voltage of 1 V is applied to the fixed fingers, and the substrate and movable fingers are grounded. Figure 3 shows the resultant torque versus angle rotated. The unit electrode is 20 μm away from the axis of rotation. Since the simulation assumes that the electrodes are perfect rectangular electrodes, it does not account for the difference in the metal coverage on the top and bottom of the SCREAM beam.

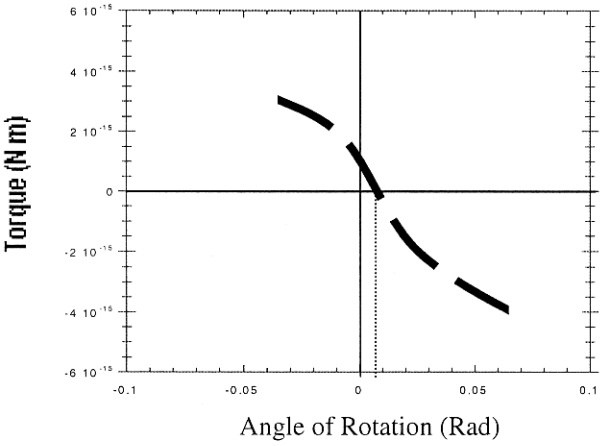

Figure 3. A plot of the levitation torque as a function of angular displacement of cantilever. The simulation consisted of one movable finger and two fixed fingers shown in Figure 2. One volt is applied to the fixed finger. The movable finger is 0.3 μm shorter than the fixed structure. It is simulated with the substrate plane infinitely far way. The simulation assumes that the electrodes are perfect rectangular conductors. The equilibrium angle is shown to be 0.008 rad.

Device Configuration

An image of the finished wafer is shown in Figure 5(a). A total of 16 dies were fabricated on three-inch wafer. The layout of a 10 x 10 array from the actuator side is shown in Figure 5(b). The actuators are individually addressable using SCREAM isolation [5]. The fabricated integrated actuator device is shown in Figure 5(c). The through-the-wafer trenches are clearly highlighted around the mirror platform by light from the other side of the wafer in Figure 5(e). There are four rigid anchors (or posts) that physically connect the actuators to the mirror underneath. During the release steps, the structures are wide enough to remain intact. The size of the integrated z-actuator is 382 μm by 250 μm; the size of mirror platform is 320 μm by 170 μm. The mirror thickness for the tested device is 100 μm; the thickness can be varied from 10 μm to couple hundred micrometers by varying the appropriate etch time and the substrate thickness. A SEM (Scanning Electron Micrograph) image of the mirror side is shown in Figure 5(d). The SCS mirror platform with a thin layer of reflective aluminum film is defined by the through-the-wafer trenches. A grating structure is shown on some elements of a 5x5 mirror array.

The width of through-the-wafer trench is 19 μm (Figure 5c). Here, the alignment window was designed wide enough to accommodate a slight misaligment. Adapting a commercial IR aligner will result in the reduction in through-the-wafer trench width. The fill factor of the mirror array is projected to increase from current 70% to almost 90% using the same device design.

Design of integrated two-depth actuators

The actuators that we have chosen to study rely on a torsion mode. While k_z of a fixed-fixed spring, a crab leg, and a folded spring configuration are proportional to h_s^3 (h_s - height of spring), the torsional spring constant k_z^{θ} is linearly related to the h_s. The torsional spring constant with a rectangular cross section is defined [4] as:

$$k_z^{\theta} = 2\beta G \frac{a_s^3 h_s}{L_c^2 L_s}$$

where a_s is the width of the torsional beams, L_s is the length of the torsion beam, L_c is the length of the torsion hinge, G is the shear modulus of rigidity of the material (G=7.96 x 10^{10} N/m^2 for Si(100)), and β is a constant determined by the aspect ratio of b/a. For the given aspect ratio of 10:1, the value of β is approximately 0.3. The vertical spring constant that is less than 1 N/m is easily optimized for the length less than 30 μm.

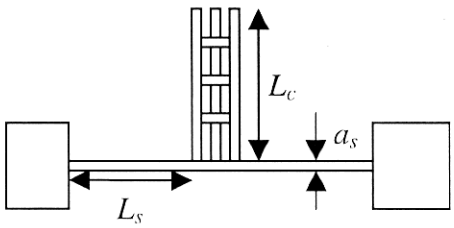

Figure 4. Schematic diagram of a torsional cantilever showing a rigid backbone structure pivoting about a centrally located support beam of length L_s, and width a_s.

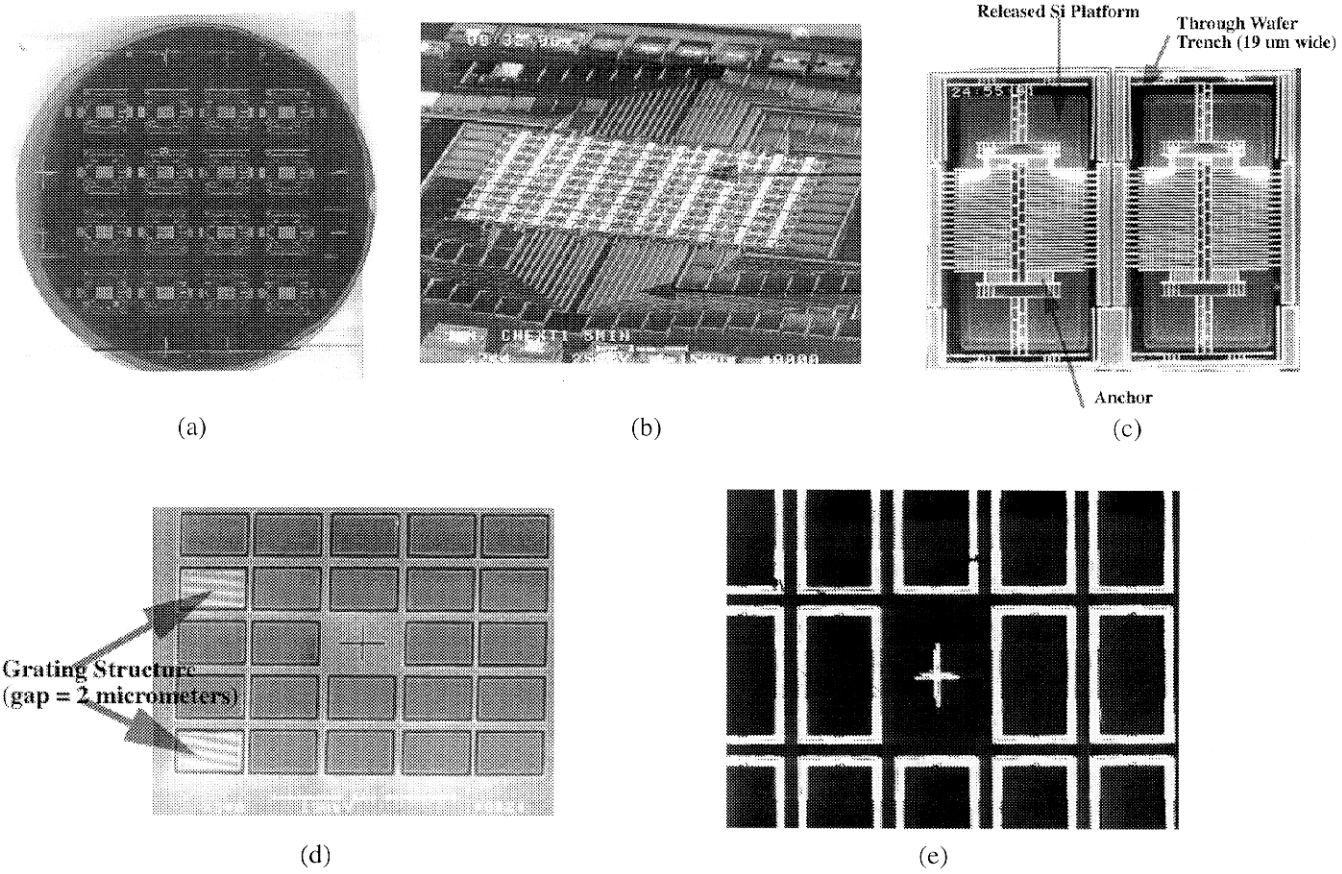

Figure 5. (a) An image of the completed wafer. Each three-inch wafer contains sixteen dies. This is a three mask process. The light is shining from the back of wafer, and the through-the-wafer trenches are shown bright. 10 x 10 arrays and 5 x 5 arrays have been fabricated (b) The overall view of a 10 x 10 micromirror array. The view is from the actuator side (the front side of a double sided polished wafer). Each actuator is individually addressable using SCREAM isolation [6]. (c) The fabricated integrated actuator device. The through-the-wafer trenches are clearly highlighted around the mirror platform. There are four rigid anchors (or posts) that physically connect the actuators to the mirror underneath. During the release steps, the structures are wide enough to remain attached to the substrate. (d) SEM image of a 5x5 micromirror array from the mirror side (back side of the wafer). The size of the integrated z-actuator is 382 μm by 250 μm; the size of mirror platform is 320 μm by 170 μm. The mirror thickness of the tested device is 100 μm. A high-aspect-ratio grating pattern with a period of 2 μm is fabricated on the flat mirror. Here, the depth of the grating is greater 70 μm. (e) The same image under the optical microscope when the light shines from the back of the wafer. The through-the-wafer trenches are shown bright.

Design of A Torsion-Based z-Motion

The torsion operation can be effectively converted into a pure z-motion by incorporating stress-relieving structures. This allows the accurate translation of mirrors out of the plane of the substrate. The schematic of a low-voltage, torsion-based integrated z-actuator is illustrated in Figure 6. Here, the backbone is divided into three parts; segments I and III make a torsional motion (no bending within each segment) in response to the vertical force generated by the two-depth actuator. Both the torsion bar and the outer portion of the stress-relieving bar (beam A) pivot in the same direction. The length expansion of this motion is accommodated by the hinging action of segments I and III. The width of the inner portion of the stress-relieving bar (beam B) is designed wider than the outer one; therefore, the inner beam does not make the same torsional motion. Instead, it acts as a rigid bar to carry a net vertical motion of segment II, the main backbone component with the movable fingers and the connections to the mirror platform underneath. This hybrid torsional spring design provides a low k_z^{θ} for deep-etched SCREAM beams. A low voltage operation is possible with a narrow, very short spring; a high mirror fill factor and a small mirror size become possible with this design. The lateral motion is greatly reduced due to very stiff lateral spring constants. Posts connect the back of the mirror platform with segment II. The torsional cantilevers cross over the through-

the-wafer trenches and are anchored to the surrounding substrate. The torsional actuator is designed with a redistributed mass and by eliminating one torsion bar at the one end of backbone.

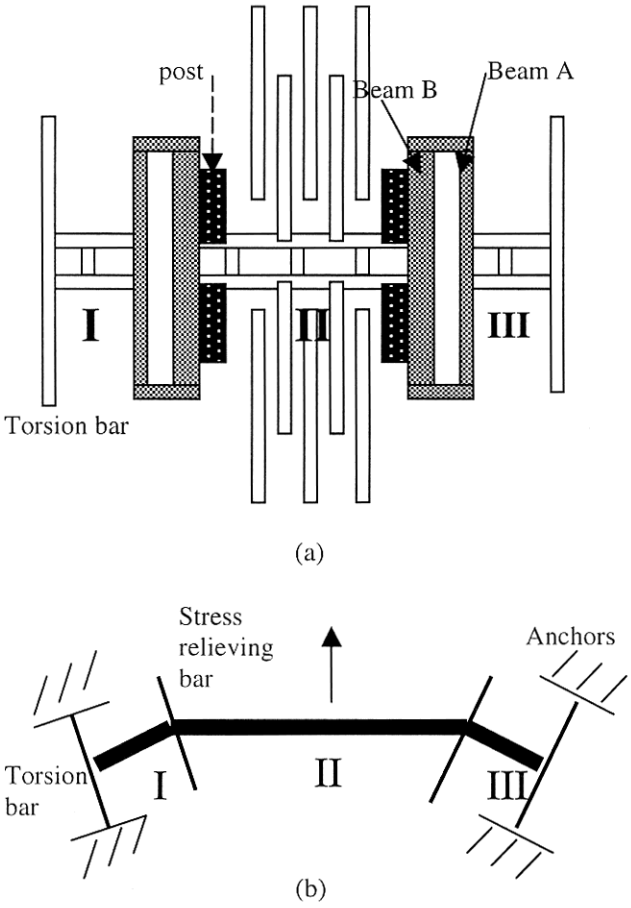

Figure 6. (a) Schematic of the integrated z-actuator system with SCS mirror platform underneath. A hybrid torsion system divides the backbone into three segments. Segment II makes a pure z-motion. The posts connect the mirror platform to segment II. (b) A cross section of the device, illustrating the z-motion operation.

Array Architecture

The design of two-depth actuator with an integrated SCS mirror platform has been discussed. The next design step is to interconnect the individual actuators to form a large array of SCS micromirrors. When the individual integrated actuators are placed in arrays, the importance of electrical connections, isolation of elements, and the overall mirror fill factor must be emphasized.

An overview of the integrated actuator is shown in Figure 5(c). Since the banks of fixed fingers are separated, the actuator configuration requires three electrical contacts for operation: one for the suspended structure and two for the fixed fingers. To increase the mirror fill factor, a suspended beam is added around the periphery of an actuator and is used to connect both banks of the fixed fingers together.

The configuration of the electrical connections for each integrated actuator is shown in Figure 7. Here, the fixed structure signal is routed horizontally from the top of the device. Since the device design is based on one level metal and no crossover is permitted, this forces the electrical contacts of the suspended structure to be routed from the bottom of the device.

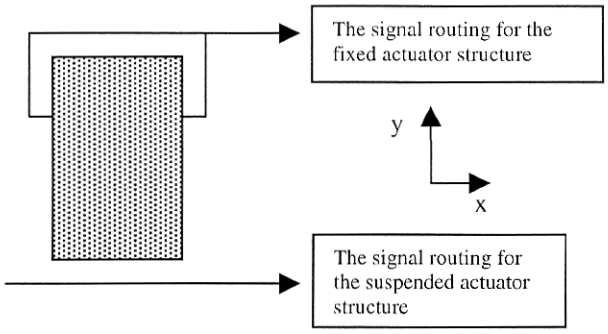

Figure 7. The electrical routing schematics at the actuator level. Only two electrical connections are required. Each signal is routed horizontally from the top and the bottom of device.

For an $n \times n$ array, $2n^2$ address lines are needed. Electrical connections to the devices on the outer edge of the array are easily made using the adjacent contact pads. However, the connections to the devices inside the array must be routed between the array elements. While each actuator needs two electrical connections, either the ground line or the suspended line can be shared with the actuators in adjacent rows. Here the actuators in the second row are a mirror image of the first row; this allows for the merging of the ground lines. This reduces the total electrical connections by approximately half. Since the mirror platform is a rectangular shape, the mirroring of the actuator does not affect the periodicity of mirror structures on the back.

The overall routing schematic is shown in Figure 8. For illustration purposes, a 6 x 6 array is considered. Here, the suspended structures in rows 2 and 3 share common address lines; the electrical connection to the suspended structures in row 2 and 3 is delivered by Vcc-1. The suspended structures in rows 4 and 5 are electrically contacted by Vcc-2. Each actuator has a unique electrical connection for the fixed structures. The fixed structure address lines from the actuators in rows 3 and 4 are routed parallel to each other. The lines from the first three columns are routed in the negative x direction, whereas the other half is routed in the positive x direction. Since the width of AA (the spacing between rows 3 and 4, for example) is largely

determined by the number of required address lines, the two-direction routing approach reduces the required spacing by half.

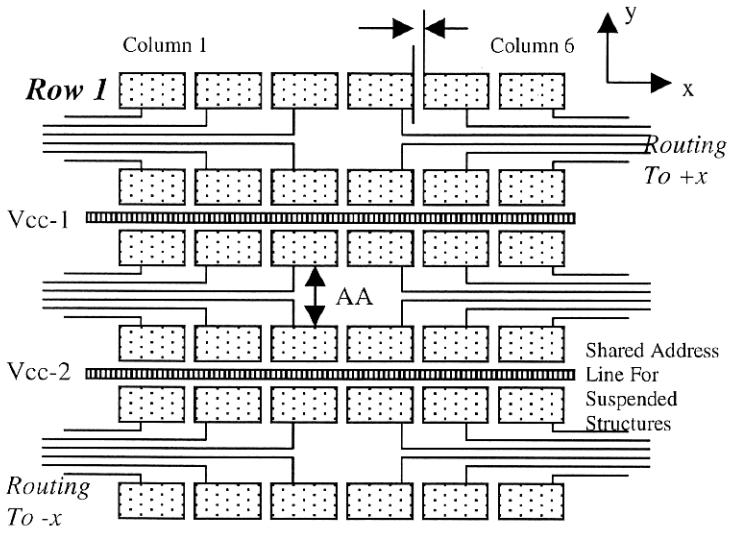

Figure 8. The schematic for the address line routing. For illustration purposes, a 6 x 6 array is considered. Here, the suspended structures in rows 2/3 and rows 4/5 share common ground lines; the electrical connection to the suspended structures in rows 2 and 3 is delivered by Vcc-1. The address line for the fixed structures in rows 1 and 2 are routed together between rows. The remaining address lines are routed in a similar fashion.

Dynamics of Integrated-actuator

In the operation of micromirror arrays, accurate control of the mirror motion is important to correct and modulate the incoming optical beam. A principal indicator of expected MEMS mirror performance is the dynamic behavior of its constituent electrostatic actuators. Their motion and frequency response characteristics are quantified in this section.

The measurement of motion at the nanometer scale is desirable since the measurement discrepancy as small as fraction of wavelength significantly changes the optical characteristics of the reflected beam. The dynamics of the micromirror device are precisely characterized using the laser vibrometry suite [7]. The natural frequency and the quality factor of the integrated actuator are accurately determined by applying an impulse voltage to the device and observing the amplitude response. The mirror thickness of the tested device is 100 μm. A 8V pulse was applied for a duration of 60 μs while the device was in atmospheric pressure. Being an underdamped system, the device will ring at its natural frequency as a result of the pulse excitation. This is shown in Figure 9. The quality factor, Q, can be determined by observing the motion of the device as its amplitude decays. Q is determined by multiplying 2π times the number of cycles required for the ringing amplitude to decrease to $e^{-1/2}$ of the initial amplitude. These values will be shown consistent with the results from the frequency-amplitude response curve.

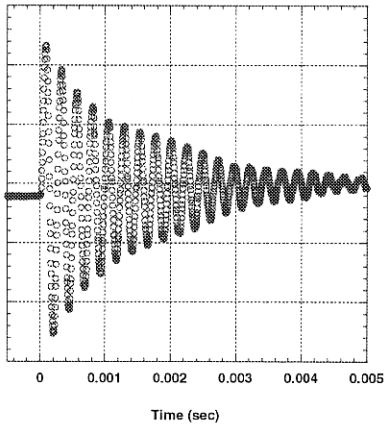

Q = 22
f_r = 4.165 KHz

(a)

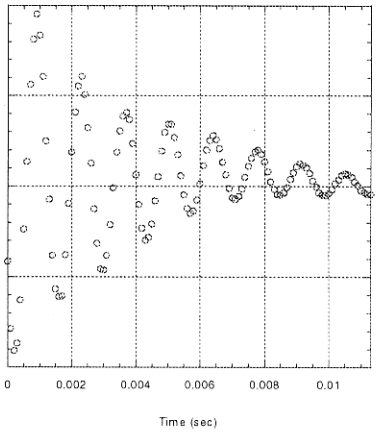

Q = 9
f_r = 740 Hz

(b)

Figure 9. The motion of integrated-actuators when exposed to a narrow pulse of 8 V amplitude for a duration of 60 μs. The size of actuator is 382 μm by 250 μm; the size of mirror platform is 320 μm by 170 μm. The mirror thickness of the tested device is 100 μm. (a) Integrated z-actuator. (b) Integrated torsional actuator.

Frequency Response Curves

Frequency response curves for the integrated actuator are shown in Figure 10. Families of response curves are obtained by incrementing the applied voltage. In conjunction with an excitation response curve (i.e., ringing plots), the critical device parameters such as damping coefficient, linear and cubic spring constants, resonant frequency, and quality factors can be extracted from the plot.

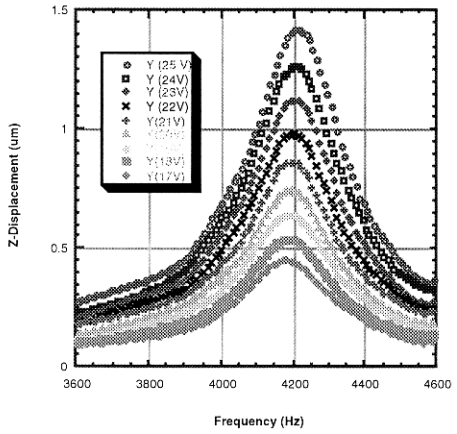

(a)

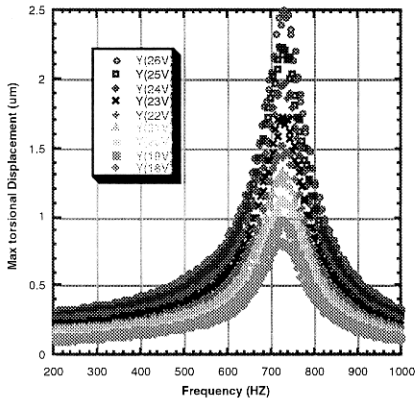

(b)

Figure 10. Frequency response of the integrated actuators in air. The measurement is done using the laser vibrometry suite. The symmetric shape of the curves indicates the linear device behavior. (a) the integrated z-actuator (b) the integrated torsional actuator.

The extracted parameters are shown in Table 1. A frequency corresponding to the highest displacement amplitude is the resonant frequency of the system. An alternate way of finding the quality factor is to look at the half-power points of the response curve. By determining the frequencies at which the amplitude of the *linear* response decreases by a factor of square root of 2 from its peak value, we can determine the quality factor. These values are consistent with the values obtained from the impulse excitation plot.

	z-actuator	torsion actuator
Linear stiffness	11 N/m	0.35 N/m
Cubic stiffness	$1.2\text{x}10^{11}$ N/m^3	$1.5\text{x}10^{10}$ N/m^3
Suspended mass	$1.6\text{x}10^{-8}$ Kg	$1.6\text{x}10^{-8}$ Kg
Resonant Frequency	4165 Hz	740 Hz
Q	22	9

Table 1. Extracted Device Parameters

The listed mechanical device parameters can be easily scaled using the design rules for the SCS through-the-wafer architecture. For example, the thickness of the fabricated mirror is 100 μm. The thickness is defined by the amount of silicon etched during the backside mirror etching and the front side actuator etching. With a reduced mass, a first-order approximation shows that the resonant frequency can be increased up to 10 KHz without changing the current design.

Array Testing: Cross Talk

The degree of cross talk between individual array element is tested in air using laser vibrometry. The dynamics of the integrated actuator is compared before and after the neighboring actuators are turned on. Figure 11(a) is the vibrometer output when 19V is applied to the integrated actuator while the surrounding actuators are off, whereas Figure 11(b) is the vibrometer output of the same actuator with 19 V signal when 20V is applied to the surrounding elements. Figure 11(c) is the frequency response comparison. The comparison indicates that there is no significant cross-talk. Also, no influence on standby actuator was observed when the surrounding actuators are turned on.

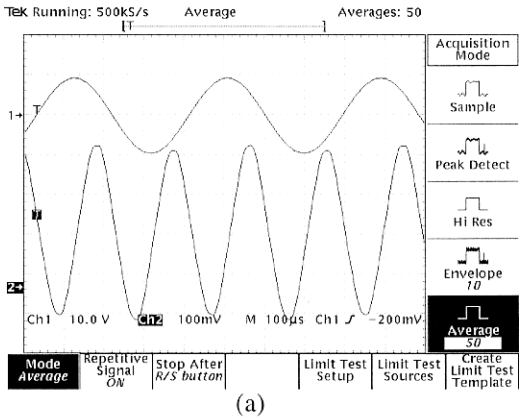

(a)

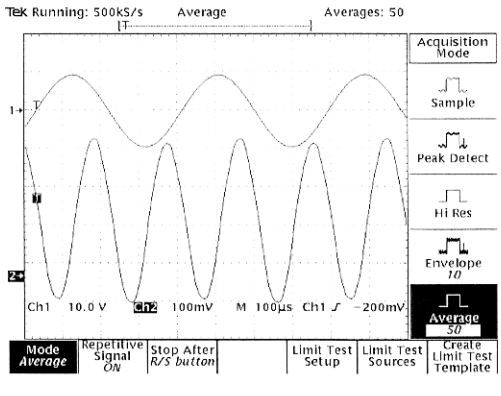

(b)

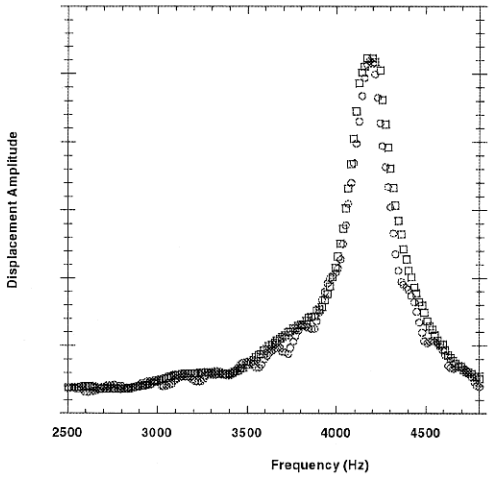

(c)

Figure 11. (a) Vibrometer output when 19V is applied to the integrated actuator while the surrounding actuators are off. (b) Vibrometer output of the same actuator with 19 V signal when the surrounding actuators are on (20V). The scale is set at 1 μm/V. (c) Comparison of frequency response curves when the surrounding element is on (circles) and the surrounding element is off (squares).

Uniformity of z-motion

The laser was focused on 10 different points along the backbone, and the corresponding z-displacement was measured. For each measurement, a total of 10 data points are collected and averaged. These points along the backbone are approximately 15 μm apart. To measure the motion at points orthogonal to the backbone, the laser spot was focused on the four posts that connect the suspended actuators to the backside mirror. As expected, the vertical motion was uniform across the mirror, and the results are plotted in Figure 12.

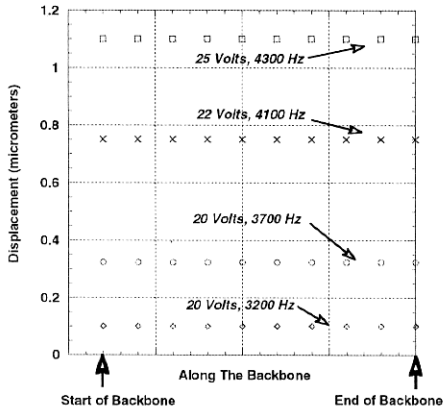

(a)

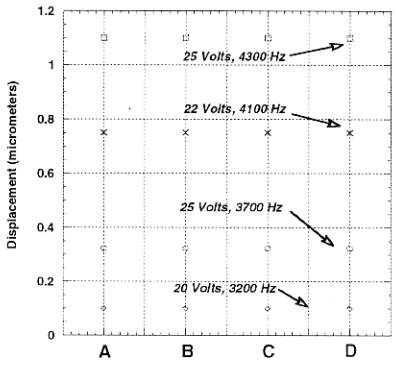

(b)

Figure 12. (a) The laser vibrometry measurement of z-motion along the backbone. For each measurement, a total of 10 data points were collected and averaged. Each representative point along the backbone is approximately 15 μm apart from the next. (b) The z-motion measurement orthogonal to the length of the backbone motion. The measurements were taken from four posts at the corners of the actuator; A=Left Upper, B=Left Lower, C=Right Upper, D=Right Lower. The plot confirms that there is no variation in the z-motion across the mirror surface.

Conclusion

10 x 10 and 5 x 5, a high mirror fill factor (> 70 %), low voltage operation (< 30 V), single crystal silicon (SCS) micromirror arrays have been designed, fabricated, and tested. Two mirror designs are presented, one for adaptive optics and the second for spatial light modulation: a pure z-motion and a torsional tilt motion. The motion is driven from the two-depth comb finger configuration. The devices are fully characterized mechanically using the laser vibrometry. The mirror surface is measured to be optically flat and smooth. The fabrication of high aspect ratio grating structures is demonstrated on the surface of SCS mirror platform.

Acknowledgments

This work is supported by DARPA. All the fabrication was performed at the Cornell Nanofabrication Facility (CNF) which is supported by the NSF, Cornell University, and Industrial affiliates. The authors would like to thank Prof. MacDonald's group members for their generous support of this research.

Reference

1. R. Mali, T. Bifano and N. Vandelli, "Development of microelectromechanical deformable mirrors for phase modulation of light", Opt. Eng. 36 (2) 542-547, Feb 1997.
2. D. Burns and V. Bright, "Designs to improve polysilicon micromirror surface topology", SPIE Vol. 3008, 100-110, 1997
3. W.C. Tang, M.G. Lim, and R.T. Howe, "Electrostatic Comb Drive Levitation and Control Method", J. Microelectromechanical Sys. 1 170-178 (1992)
4. S.A. Miller, "Microelectromechanical Scanning Probe Instruments For Array Architectures", Ph.D. Thesis, Cornell University, 1998.
5. Kimberly L. Turner, Scott A. Miller, Peter G. Hartwell, Noel C. MacDonald, Steven H. Strogatz, and Scott G. Adams, "Five Parametric Resonances in a Microelectromechanical System", *NATURE, Vol 396, pp. 149-152, November 12, 1998.*
6. K.A. Shaw, Z.L.Zhang, and N.C. MacDonald, "SCREAM I: A single mask, single-crystal silicon, reactive ion etch process for microelectromechanical structures", Sensors and Actuators A 40, 63-70 (1994).
7. K. Turner, P. Hartwell, and N.C. MacDonald, "Mult-Dimensional MEMS Motion Characterization using Laser Vibrometry", Transducers 99, 1144-1147, Sendia Japan.